Eur. Phys. J. AP **5**, 277–281 (1999)

THE EUROPEAN PHYSICAL JOURNAL APPLIED PHYSICS

Spectroscopic study of resonant dielectric structures in near-field*

S. Davy, D. Barchiesi[a], M. Spajer, and D. Courjon

Laboratoire d'Optique P.M. Duffieux[b], Université de Franche-Comté, Institut des Microtechniques, 25030 Besançon Cedex, France

Received: 2 July 1998 / Revised: 29 September 1998 / Accepted: 29 October 1998

Abstract. Gratings can be considered as resonant structures in near-field. The enhancement of the intensity recorded by Scanning Near-Field Optical Microscopes (SNOM) is due to interferences in relation with the ratio of the wavelength to the product of the optical index by the period of the grating. We discuss the effect of this ratio (in the range 0.9, 1.1) on the intensity patterns. The influence of the polarization on near-field data is analyzed in both theoretical computations and experimental result.

PACS. 07.79.Fc Near-field scanning optical microscopes

1 Introduction

Scanning Near-Field Optical Microscopy (SNOM) has opened the way to local investigation at a subwavelength scale. It is more than a simple imaging device, since it allows the transposition of many far-field optical techniques to the near-field. Near-field spectroscopy is probably one of the best example of such a successful transposition and it is partly responsible *for* the growing number of teams and articles in near-field activity. Concerning history, the first near-field fluorescence experiment has been carried out by Betzig *et al.* in 1986 [1]. Some works reported in references [2,3] describe the use of this technique for single molecule detection. Sometimes, near-field spectroscopy is not carried out for measuring the light intensity but rather for determining the lifetime decay of fluorescence [4]. More generally, SNOM is a very powerful tool for multiwavelength analysis. We focus here our interest on the spectroscopic behavior of a periodic structure or grating which can exhibit resonant properties. One of our aims is to estimate whether the depolarization of the light is mainly due to the sample or due to the tip. We study the illumination properties and finally we discuss the spectroscopic behavior of the near-field in the case of a periodic structure.

2 Setup, sample and model description

The principle of the experiment is based upon a reflection SNOM (R-SNOM) [5] and is depicted in Figure 1: the sample is scanned by a tapered fiber obtained by means of a commercial micro-pipette puller. Such a probe has typically 80 nm tip diameter and can be coated in a vacuum chamber with a 100 nm thick aluminum layer (except the extremity). The tip is maintained a few nanometers from the sample surface by means of a shear-force mechanism [6] which allows to record the sample topography. In such a microscope, the tip is both a nano-source and a nano-receiver. This involves the use of non metal coated tip in order to ensure a satisfying optical signal. The illumination source is a titanium-sapphire tunable laser (Spectra Physics 3900s) whose wavelength can be tuned from 700 to 850 nm and from 850 to 1000 nm with two different set of cavity mirrors. When pumped by a 8 W Ar laser, it supplies a maximum power of 1 W for $\lambda = 800$ nm which drops to 100 mW for $\lambda = 950$ nm. After injection into the optical fiber, the final beam polarization is unknown because we did not use polarization maintaining fiber. The chosen solution for controlling the polarization at the extremity of the probe was using two

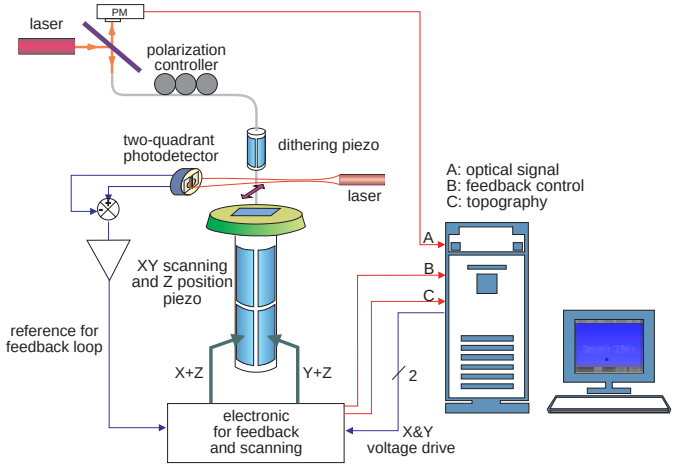

Fig. 1. R-SNOM principle.

* This paper was presented at the special CFMCP colloquium held at Strasbourg-Illkirch the July 1st-3rd, 1998.

[a] e-mail: dominique.barchiesi@univ-fcomte.fr

[b] CNRS UMR 6603

Lefebvre loops. The sample is a matrix of holes on a glass substrate. The holes are 300 nm wide, 300 nm deep and 600 nm spaced. The whole matrix is around 50 μm$\times$50 μm large. The optical index of the glass is 1.46 and varies slowly in the considered spectral range.

The model we used for describing the diffraction by the grating was used previously to explain the R-SNOM working in constant height mode and the influence of the distance between the tip and the sample [7]. The calculation of the electromagnetic field is deduced from the Maxwell equations and the boundary conditions on the sample. The main point is the Rayleigh hypothesis which supposes the validity of the plane wave spectrum in the region of sample corrugations. Therefore two types of algorithms can be applied to compute the electromagnetic field which is diffracted by the sample. The first one is the no-perturbation scheme which we applied in [7]. A three-dimensional perturbation algorithm, completely analytical, is detailed and applied to coated nano-sources in [8]. The last one leads to rapid computation and is suitable for spectroscopic studies. On the other hand, some conditions have to be fulfill to insure good accuracy. The first one concerns the ratio smallness of the height of the roughness to the period, to permit a perturbation scheme. The second one is the smallness of the ratio of the height to the lateral size of the sample. In that context we showed that the effect of the periodicity of the sample could be neglected with some care, by comparing our results with results obtained by using a direct space model [9]. On the contrary, in this paper, we use a similar method in the domain of validity of the model. For this purpose, we consider more than one period (between 2 and 6) of the 2D grating in each direction to verify the first condition. Consequently, the description of the sample is a little more crude for a given number of harmonics, but it is not crucial as we will show. The second condition is less critical as shown in [10]. It has to be noticed that we will consider in a further section, a polarized incident plane wave and we calculate the intensity in each point in a constant plane a few nanometers above the sample. Three hypothesis are therefore introduced:

- the dielectric tip does not depolarize the incident light, and the depolarization of the light, if any is only due to the diffraction by the sample;
- the dielectric tip acts like a passive probe. It detects the square modulus of the electric field at the very end of the tip, without integrating the signal nor *influencing* the detected signal;
- the shear-force feedback perturbs only locally the detected optical signal, when the tip enters the hole of the grating.

These three points have been intensively discussed for the last years and they will be verified by comparing theory and experiments in a spectroscopic experiment.

3 Polarization effects

The first optical images we have recorded exhibit some fringe pattern. These fringes can rotate from one image to another after a polarization rotation with the Lefebvre loops. According to numerical computations, the fringes direction is perpendicular to the **E** direction.

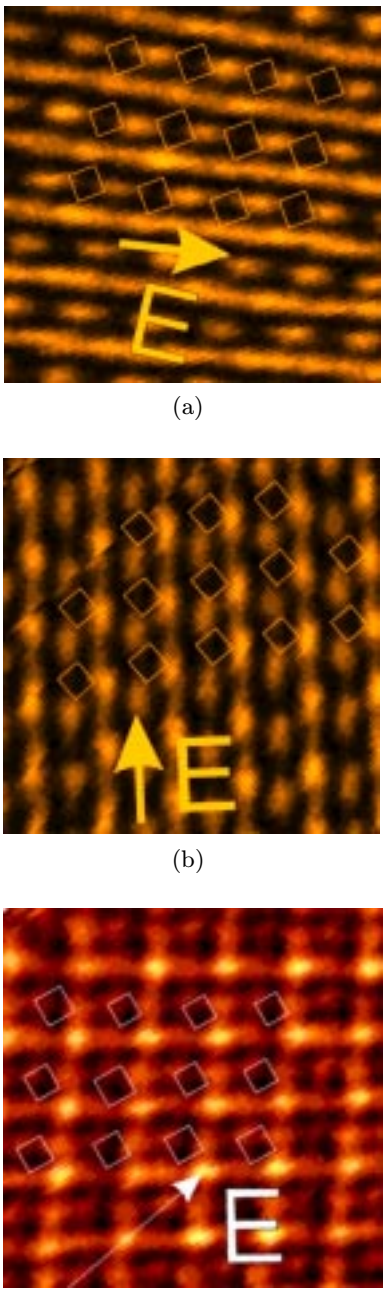

(a)

(b)

(c)

Fig. 2. Optical images with different polarization angles (3.7$\times$ 3.7 μm, $\lambda = 782$ nm).

The basic principle of Scanning Optical Microscopes is the electromagnetic interaction between the tip and the sample. In a first approach we figure out three sources of depolarization in R-SNOM: the tip by the illumination process, the sample and the tip by the detection process. Figures 2 and 3 show the agreement between the behavior of a polarized incident plane wave and a non polarized

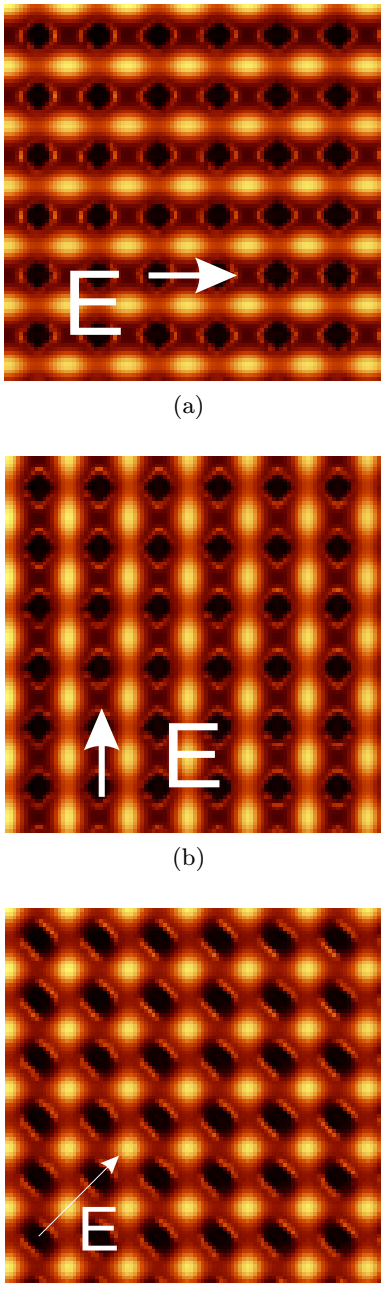

(a)

(b)

(c)

Fig. 3. Numerical computation (3.7×3.7 μm, $\lambda = 782$ nm).

detection, and the experimental illumination and detection process. *Thanks to the topographical image, we can localize the holes position in the optical image.* Therefore, we superimpressed the location of the square holes (white squares) on the optical image in Figure 2. Thus we can conclude that the depolarization induced by the dielectric tip can be neglected in the image formation process. The effect of the tip seems to be a widening of the local confinement of the intensity on the neighborhood of the edges of the holes. The shade on one side of each hole, in the direction of **E**, is readily seen in both theoretical (Fig. 4a)

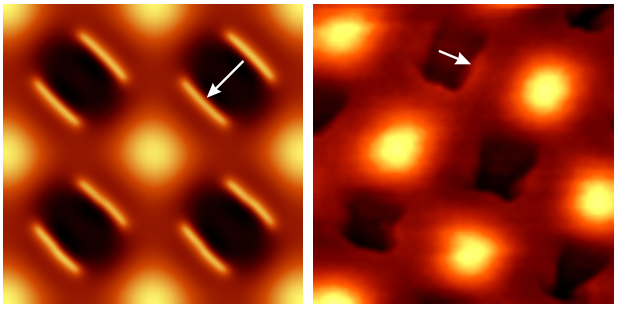

(a) (b)

Fig. 4. Edge enhancement (white arrows) in both theoretical and experimental images, $\lambda = 850$ nm, in both image the period of the holes is 600 nm. (a) Theoretical (1.2×1.2 μm), (b) experimental (1.5×1.5 μm).

and experimental (Fig. 4b) images. The fringe patterns is governed by the same law: the fringe appears between the grating holes.

When the electric field is along the diagonal of each square pattern the two perpendicular fringe patterns are superimposed, leading to a single enhancement between the hole, whose location is sensitive to the electric field direction.

Another remark should be made on the hypothesis of the dipolar tip. The scanning step is half the tip end size (about 50 nm). The effect of signal integration by the tip can be as wide as 150 nm. Consequently, the weak intensity enhancement at the edges of the hole is smoothed.

We can also point out the relationship between the model of detection and the used tip. The distance d between the sample and the plane where the intensity is calculated (30 nm) is optimized to obtain better contrast of the fringes between the holes. If the distance is less, the holes are more contrasting and the fringes are less visible because the weight of evanescent waves corresponding to high spatial frequencies is greater when tip-sample distance decrease. Otherwise, if d is greater than 30 nm, the fringes are faded, their contrast decreases, because the amplitude of the corresponding first order of diffraction diminishes. In the experimental condition, the tip-sample distance is determined by shear-force mechanism. This mechanism is not well-known, but some approach curves show that in this case the tip-sample distance is smaller than 10 nm. Therefore, the comparison with the previous theoretical remarks induces that the detection is not led only by the very end of the tip but probably by a more than 30 nm long active region.

4 Spectroscopic study

By varying the incident wavelength, a well-known change of intensity can be observed. The first change occurs when the wavelength is equal to the period a of the grating. In normal incidence (in R-SNOM), the first diffracted order

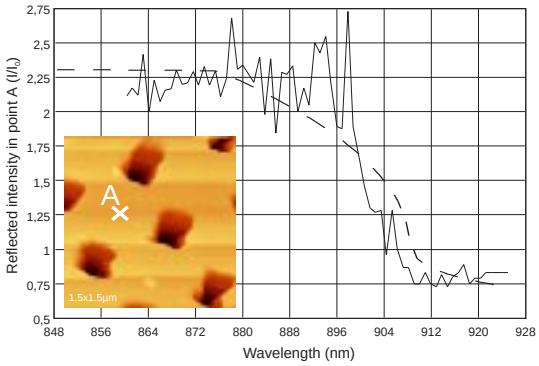

Fig. 5. Theoretical and experimental spectrum of the reflected intensity in point A.

propagates or becomes evanescent. The same type of behavior is observed when λ crosses the na limit, n being the index of the grating. It was not possible to study the transition at $\lambda = a$ because we do not have any tunable laser around 600 nm. The studied site is located between four holes and the polarization angle is 45° *versus* the line holes direction. We must take into account the "spectroscopic" behavior of the whole microscope: the output power of the lasers, the photomultiplier response are not constant respect to the wavelength. Therefore, the plane glass spectrum has been used as a reference. The spectrum in point A has been recorded and we have normalized the data according to the plane glass ones. The curve is the solid line in Figure 5. The Y axis unity is the ratio I/I_0 where I is the measured reflected intensity in point A and I_0 the reflected intensity on plane glass. In the same figure, the calculate intensity has been reported for the same point (dashed line). In spite of the raw aspect of the experimental data, we observe a good agreement with numerical computation concerning the transition between homogeneous mode and evanescent mode. We can see that for $\lambda < na$, I is two times greater than expected on plane glass.

The model developed in [8] leads to analytical solution of the problem of diffraction by a 3D multilayer structure. The electromagnetic field is calculated by involving the boundary conditions on the diffractive structure and for simplicity, Rayleigh hypothesis. To match the boundary conditions, the plane wave expansion is used in the region of corrugation as out of this domain. The first expansion is not rigorously valid but enables the analytical calculations. Various comparison in far field and in near-field [9] showed the good agreement between rigorous theories, experiment and Rayleigh hypothesis based theory, if the ratio of the roughness of the diffractive structure to the wavelength is small enough [7]. The electromagnetic field can be calculated from a perturbation scheme using the profile as perturbation. For example, the electric field can be written:

$$\mathbf{E} = \mathbf{E}_0 + \mathbf{E}_{\text{diff}} = \mathbf{E}_0 + \hat{f}\mathbf{M}_1 + \hat{f}^2\mathbf{M}_2 + \ldots \quad (1)$$

In this study, we focus on the linear terms of the diffracted electromagnetic field as a function of the profile spectrum. Above all, the diffracted field in the medium of the incident light is related to the R-SNOM detected signal. The scanned sample is of index n. The calculation of the diffracted field Fourier spectrum $(E_{\text{d}x}, E_{\text{d}y}, E_{\text{d}z})$ (in medium of index 1) is given as a function of the incident field (in the same medium) with normal incidence $(E_{\text{i}x}, E_{\text{i}y}, 0)$ by:

$$\begin{pmatrix} E_{\text{d}x} \\ E_{\text{d}y} \\ E_{\text{d}z} \end{pmatrix} = \hat{f}\frac{2\jmath(1-n^2)w_1}{(w_1+w_2)(n^2wg_1+wg_2)} \times \begin{pmatrix} vg^2+wg_1wg_2 & -ugvg \\ -ugvg & ug^2+wg_1wg_2 \\ ugwg_2 & vgwg_2 \end{pmatrix} \begin{pmatrix} E_{\text{i}x} \\ E_{\text{i}y} \end{pmatrix}. \quad (2)$$

For the R-SNOM simulation, the x, y components of the diffracted wave vector (in the sample mean plane) are given by:

$$ug = p\frac{2\pi}{a_x}, \quad (3)$$

$$vg = r\frac{2\pi}{a_y}, \quad (4)$$

$$wg_2 = \sqrt{\frac{\omega^2}{c^2}n(\lambda)^2 - ug^2 - vg^2}, \quad (5)$$

with p and r integers. The sample is supposed to be periodical with period a_x along x axis and period a_y along y axis. In the R-SNOM simulation, the incident wave vector verifies $u = 0$, $v = 0$ and $w_1 = \omega/c$. The illumination is supposed to be a plane wave. The corresponding z component of the wavevector in the sample is $w_2 = n\omega/c$. wg can be real (homogeneous wave) or imaginary (evanescent wave). The incident wavevector components verify the dispersion equation:

$$u^2 + v^2 + w_1^2 = \frac{\omega^2}{c^2}, \quad (6)$$

$$u^2 + v^2 + w_2^2 = \frac{\omega^2}{c^2}n^2. \quad (7)$$

w being the component which is normal to the sample mean plane. The diffracted wavevectors verify:

$$ug^2 + vg^2 + wg_1^2 = \frac{\omega^2}{c^2} \quad (8)$$

$$ug^2 + vg^2 + wg_2^2 = \frac{\omega^2}{c^2}n^2. \quad (9)$$

The detected intensity $I(x, y, z)$ is supposed to be the square modulus of the Fourier transform of the previous electric field, including a propagation or exponential decay as a function of the distance of detection z

$$I(x,y,z) = \left| \sum_{p=-\infty}^{p=+\infty} \sum_{r=-\infty}^{r=+\infty} \mathbf{E}(p,r) \exp \jmath(ugx + vgy - wg_1 z) \right|^2. \quad (10)$$

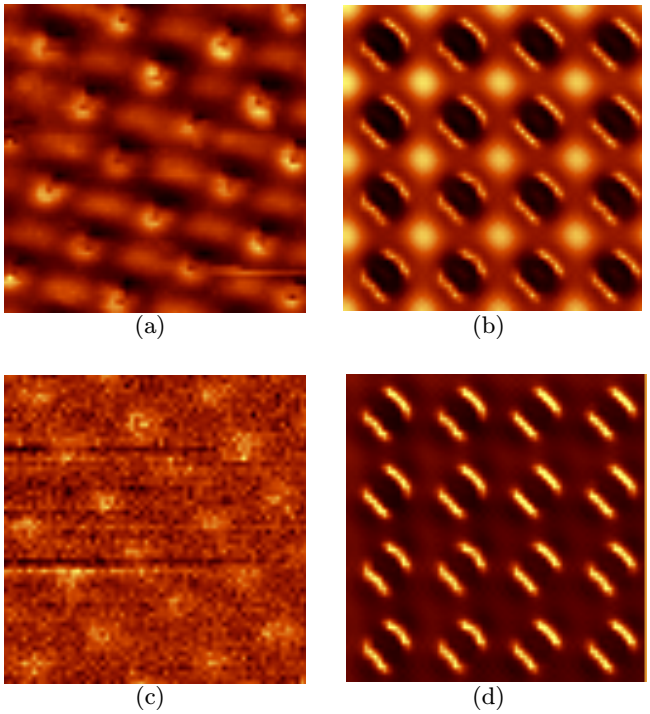

Fig. 6. Experimental and theoretical images on the left and on the right of the limit na. (a) $\lambda = 850$ nm, 3×3 μm, (b) $\lambda = 850$ nm, computed image, (c) $\lambda = 925$ nm, (d) $\lambda = 925$ nm, computed image.

The exponential decay appears when the diffracted mode is evanescent, *i.e.* when wg_1 is purely imaginary. According to the ratio of λ to period a, w can be real or imaginary. For simplicity, we introduce $\lambda = n(a \pm \delta\lambda)$:

$$wg_2(p = 1, r = 0) = n\frac{\omega}{c}\frac{\sqrt{\delta\lambda}}{a}\sqrt{\mp 2a - \delta\lambda}. \qquad (11)$$

Therefore, the terms of the matrix is either real or imaginary like wg_2. This property implies that the corresponding contribution of the electric field contains a supplementary phase factor $\exp(\pi/2)$ (especially for the first order of diffraction) with respect to the Fresnel wave (the zero order of diffraction), if the wavelength is greater than the limit na. Otherwise the Fresnel wave and the first order have the same phase. This leads to a higher contribution of the first order of diffraction if $\lambda < na$.

We obtained an efficiency of this order respectively equal the half of the zero order if $\lambda = 850$ nm, whereas it is only 1/6 of the efficiency of the Fresnel wave for $\lambda = 925$ nm. This fact can explain the fading of fringe pattern in Figures 6c and 6d. If the wavelength is greater than the limit na, the "resonance" of the first order diffracted harmonic disappears and the image looks more isotropic. The near-field information is less perturbed. The fringes which are obtained if $\lambda < na$ are perpendicular to the electric field and have period a. They correspond to the magnification of the first diffracted harmonic of the grating.

5 Conclusion

We have studied the problem of depolarization and we have interpreted a spectroscopic study on a biperiodic grating. We have shown that the R-SNOM tip-induced-depolarization is much smaller than the depolarization due to the light-sample interaction. We have interpreted the formation of images when the wavelength varies, especially the presence of fringes patterns. The theoretical study of the diffraction by a dielectric deep grating can help to interpret experimental results and the relevant phenomena have been described by means of a perturbation method, at the very limit of its mathematical range of validity. In further studies we will study more carefully the enhancement of the intensity near the na limit and we will determine how this effect can be related to other resonance of structure, like photonic bandgaps [11].

References

1. A. Harootunian, E. Betzig, M. Isaacson, A. Lewis, Appl. Phys. Lett. **49**, 674 (1986).
2. A. Meixner, D. Zeisel, M.A. Boop, G. Tarrach, Opt. Eng. **34**, 2324 (1995).
3. R. Chang, W. Fann, H. Lin, Appl. Phys. Lett. **69**, 2338 (1996).
4. T. Pagnot, D. Barchiesi, D. van Labeke, C. Pieralli, Opt. Lett. **22**, 120 (1997).
5. D. Courjon, J.M. Vigoureux, M. Spajer, K. Sarayeddine, S. Leblanc, Appl. Opt. **29**, 3734 (1990).
6. E. Betzig, P.L. Finn, J.S. Weiner, Appl. Phys. Lett. **60**, 2484 (1992).
7. D. Barchiesi, O. Bergossi, M. Spajer, Ch. Pieralli, Ultramicroscopy **71**, 361 (1998).
8. D. Barchiesi, Opt. Commun. **126**, 7 (1996).
9. D. Barchiesi, Ch. Girard, O.J.F. Martin, D. van Labeke, D. Courjon, Phys. Rev. E **54**, 4285 (1996).
10. E. Popov, L. Mashev, Optica Acta **33**, 593 (1986).
11. A. Sentenac, J.J. Greffet, F. Pincemin, J. Opt. Soc. Am. B **14**, 339 (1997).